Fracture and Local Buckling Behaviour of Stainless Steel Circular Hollow Sections Subjected to Eccentric Tension

Ou Zhao, V.V.K. Jeyapragasam and Yating Liang

Nanyang Technological University, Singapore

Abstract

The fracture and local buckling behaviour of stainless steel circular hollow sections (CHS) under combined tension and bending moment is investigated, based on numerical modelling. A total of 750 numerical models with various cross-section diameters and thicknesses and loading eccentricities were developed. The numerical results were carefully analysed and compared with the resistance predictions determined from the existing international design standards, indicating undue conservatism. The continuous strength method, which rationally considers strain hardening in the calculation of cross-section resistances, is extended to cover the design of stainless steel CHS under eccentric tension, and shown to yield accurate resistance predictions.

Keywords

Circular hollow section; Design analysis; Eccentric tension; Fracture; Local buckling; Numerical modelling; Stainless steel

1 Introduction

Structural stainless steel possesses better aesthetic appeal, more favourable material properties and higher corrosion and fire resistances over the conventional carbon steel, and thus has been increasingly used in civil and offshore engineering. For the design of stainless steel structures, the existing design standards were generally developed by mirroring the corresponding carbon steel design provisions without accounting for the distinctive nonlinear stress–strain response and strain hardening behaviour of stainless steel, and therefore resulted in inaccurate design. In order to overcome these drawbacks, in-depth experimental and numerical studies into the mechanical behaviour of stainless steel materials and members have been conducted, and more accurate and efficient design rules have been developed. As part of a wider study that is currently being carried out by the authors to investigate the structural performance of stainless steel cross-sections and members subjected to combined loading, this paper focuses on the numerical modelling and design of stainless steel circular hollow sections (CHS) under combined tension and bending moment. Previous relevant studies are briefly reviewed herein. Zhao et al.[1–3] and Arrayago and Real[4] conducted a series of eccentrically loaded stub column tests on stainless steel CHS and square and rectangular hollow sections (SHS and RHS), to investigate their local buckling behaviour under combined actions of axial compression and bending moment. Comparisons of the combined loading test results against the codified resistance predictions generally indicated a high level of conservatism in the current stainless steel design standards, which mainly stemmed from the neglect of strain hardening. Improved deign approaches were then developed by Zhao et al.[2,5,6], based on the deformation-based continuous strength method (CSM)[7–10], which account for strain hardening in the determination of cross-section resistances and are shown to yield substantially more accurate design resistance predictions. A series of experimental and numerical studies have been carried out on stainless steel CHS[11] and SHS and RHS[12–14] beam-columns, in order to investigate their global stability under combined compression and uniform (first order) bending moment. Stainless steel SHS and RHS beam-column tests under moment gradients were conducted by Zhao et al.[15] to study their interaction buckling behaviour under combined axial compressive load and non-uniform (first-order) bending moment. The obtained test and numerical results generally revealed that the existing codified beam-column interaction curves led to scattered strength predictions, which principally resulted from the inaccurate end points and shape of the design curves. Revised stainless steel beam-column design interaction formulae have been proposed by Greiner and Kettler[16] and Zhao et al.[17].

The present study focuses on the numerical modelling and design of stainless steel CHS subjected to combined actions of axial tension and bending moment. Finite element (FE) simulations of both the local buckling behaviour and tensile fracture of stainless steel CHS under eccentric tension are firstly described. The developed FE models were validated against the previous eccentric tension tests on CHS, and then employed to conduct parametric studies to generate structural performance data over a broad range of stainless steel grades, cross-section geometries and loading combinations. The numerically derived results were utilised to assess the accuracy of the existing design rules for stainless steel CHS under combined tension and bending moment, given in the European code EN 1993-1-4[18], American specification SEI/ASCE-8[19] and Australian/New Zealand standard AS/NZS 4673[20]. Improved design approaches were also proposed through extending the deformation-based continuous strength method to the case of combined loading (tension and bending moment). The accuracy and reliability of the new design proposal were then assessed against 750 numerical results.

Paper not presented

2 Numerical Modelling

2.1 General

A numerical modelling programme was carried out by means of the finite element analysis package ABAQUS[21], to simulate the previous eccentric tension tests on CHS, and to conduct parametric studies to generate structural performance data over a broad range of stainless steel grades, cross-section geometries and loading combinations. The detailed numerical modelling of the material behaviour, boundary conditions and initial local geometric imperfections was described in the following sub-sections.

2.2 Material modelling

The two-stage Ramberg–Osgood material model[22–25], which is an extension of the basic Ramberg–Osgood formulation[22,23], with developments by Mirambell and Real[24] and Rasmussen[25], was adopted to represent the engineering stress–strain responses derived from tensile coupon tests, as given by Eq. (1), where ε and σ are the nominal strain and stress, respectively, $\sigma_{0.2}$ is the 0.2% proof stress, σ_u is the ultimate stress, $\varepsilon_{0.2}$ is the total strain corresponding to the 0.2% proof stress, E is the initial Young's modulus, $E_{0.2}$ is the tangent modulus at the 0.2% proof stress point ($\varepsilon_{0.2}$, $\sigma_{0.2}$), and n and m are the strain hardening exponents characterising the degree of nonlinearity of the stress–strain curve below and beyond the 0.2% proof stress. Previous experimental studies[26, 27] indicated that the two-stage Ramberg–Osgood material model yields an excellent representation of the full nominal (engineering) stress–strain curves up to the ultimate stress σ_u. Since ABAQUS requires the material properties to be specified in the form of true stress and true plastic strain, the engineering stress–strain curves, represented by Eq. (1), were converted into the true stress–true plastic strain curves, according to Eqs (2) and (3), in which σ_{true} is the true stress, ε_{ln}^{pl} is the logarithmic plastic strain, and σ_{nom} and ε_{nom} are the nominal (engineering) stress and strain, respectively. Note that the true stress–true plastic strain curve, converted from the two-stage Ramberg–Osgood material model, was used up to the true ultimate stress $\sigma_{u,true}$.

$$\varepsilon = \begin{cases} \dfrac{\sigma}{E} + 0.002\left(\dfrac{\sigma}{\sigma_{0.2}}\right)^n & \text{for } \sigma \le \sigma_{0.2} \\ \dfrac{\sigma - \sigma_{0.2}}{E_{0.2}} + \varepsilon_u\left(\dfrac{\sigma - \sigma_{0.2}}{\sigma_u - \sigma_{0.2}}\right)^m + \varepsilon_{0.2} & \text{for } \sigma_{0.2} < \sigma \le \sigma_u \end{cases} \tag{1}$$

$$\sigma_{true} = \sigma_{nom}(1 + \varepsilon_{nom}) \tag{2}$$

$$\varepsilon_{ln}^{pl} = ln(1 + \varepsilon_{nom}) - \frac{\sigma_{true}}{E} \tag{3}$$

With regards to the numerical modelling of structural members susceptible to local buckling and global instability, a true stress–true plastic strain curve up to the true ultimate stress is appropriate for this purpose, while for the numerical simulation of structural members failing by tensile fracture, a true stress–true plastic strain curve beyond the true ultimate stress until fracture is also required, in order to fully capture the fracture behaviour. Note that in the material tensile coupon tests, necking generally starts at the engineering ultimate stress point[28, 29], and then deformations become localised. The elongations of the tensile coupons are measured using extensometers, which can only record the average elongation over the gauge length rather than the localised elongation in the necked region. Therefore, the measured engineering stress–strain curve beyond the ultimate stress until fracture does not represent the actual material response, and cannot be directly used and converted into the true stress–true plastic strain curve for inputting into ABAQUS. The well-established power law expression for ductile metallic materials[28] was used herein to determine the true stress–true plastic strain curve beyond the true ultimate stress until fracture, as given by Eq. (4), where $\sigma_{frac,true}$ is the true fracture stress, K is strength constant and p is the strain hardening parameter. The values of K and p were obtained through a (linear) regression fit of Eq. (4) to the logarithmic values of the true stresses (up to true ultimate stress) and the corresponding true plastic strains; the slope and the vertical intercept of the linear regression line were taken as the values of K and p, respectively. Upon determination of the strength constant K and the strain hardening parameter p, the true stress–true plastic strain curve beyond the true ultimate stress until fracture can be derived.

$$\sigma_{true} = K\left(\varepsilon_{true}^{pl}\right)^p \qquad \text{for } \sigma_{u,true} < \sigma_{true} \le \sigma_{frac,true} \tag{4}$$

Previous tensile coupon tests on structural carbon steel and stainless steel indicated that the true fracture strains range from 80% to 120%. An average value of 100% was recommended by Salih et al.[30] as the fracture strain point in the material modelling, which is also adopted herein. In summary, the true stress–true plastic strain curve up to the true ultimate stress was converted from the two-stage Ramberg–Osgood material model[22–25], while the power law expression[28], as defined by Eq. (4), was used to derive the true stress–true plastic strain curve beyond the true ultimate stress until the fracture strain of 100%.

2.3 Basic modelling assumptions

The four-noded doubly curved shell element with reduced integration, S4R, was employed to simulate the structural performance of stainless steel thin-walled circular hollow sections under eccentric tension. A uniform mesh size equal to the material thickness was assigned to the FE models along both the longitudinal and circumferential directions. Since the numerical models were symmetric with respect to the mid-height plane and the plane perpendicular to the buckling axis, only half of the member length and cross-section was modelled, in order to reduce computational time. The end section of the FE model was coupled to an eccentric reference point, allowing longitudinal translation as well as rotation about the buckling axis, in order to simulate the pin-ended boundary conditions. An axial tensile load was then applied to the numerical models through the eccentric reference point, resulting in the combined actions of axial tensile force and bending moment to the members. The incorporated initial local geometric imperfection pattern was assumed to be of the lowest elastic local buckling mode shape under pure compression, with the imperfection amplitude equal to 1/100 of the material thickness[6]. Finally, static Riks analysis, accounting for both material and geometric nonlinearity, was conducted to simulate the full load–deformation histories of CHS under combined tension and bending moment.

2.4 Validation of numerical models

There have been no experimental investigations into the structural performance of stainless steel CHS subjected to combined actions of tension and bending moment. Therefore, the developed finite element models were validated against the corresponding eccentric tension tests on carbon steel CHS, as reported in Li et al.[31]. The only difference between the numerical simulations of stainless steel and carbon steel CHS subjected to eccentric tension lies in the material modelling prior to the true (or engineering) ultimate stress. While the two-stage Ramberg–Osgood material model was used for stainless steel, a multi-linear material model[31] was adopted to represent the measured carbon steel material stress–strain response up to the ultimate stress, which was then converted into the true stress–true plastic strain curve for inputting into ABAQUS.

Comparisons between the experimental and numerical load–deformation histories are shown in Fig. 1, indicating that the initial stiffness and the general shape of the experimental load–end elongation curves are fully captured by the numerical modelling. Therefore, the developed finite element models are capable of simulating the experimental responses of carbon steel CHS stub columns subjected to eccentric tension, and are thus considered to be validated.

2.5 Parametric studies

Parametric studies were then performed, using the validated FE models, to generate structural performance data on stainless steel CHS subjected to eccentric tension. In the present parametric studies, the (engineering) material properties were taken from the previous eccentric compression tests on stainless steel CHS, SHS and RHS, as shown in Table 1, and the incorporated initial local geometric imperfection pattern was assumed to be of the lowest elastic local buckling mode shape under pure compression, with the imperfection amplitude equal to 1/100 of the material thickness[6]. Regarding the geometric properties of the modelled CHS, the outer diameter D was set equal to 150 mm, while the cross-section thicknesses t were varied between 3 mm and 16 mm. The resulting modelled CHS covered Class 1–3 (non-slender) cross-sections, according to the slenderness limits in EN 1993-1-4[18]. The model length was equal to three times the outer cross-section diameter. The initial loading eccentricities e_0 were varied between 5 mm and 500 mm, leading to a broad range of loading combinations to be considered. For CHS stub columns loaded at large eccentricities, where the bending effect is dominant, the overall failure is governed by local buckling under bending, and a sharply defined ultimate load can be obtained, while for CHS stub columns loaded at relatively small eccentricities, the overall failure is due to tensile fracture and no peak load is evident. Previous numerical studies on carbon steel and stainless steel bolted connections composed of flat sheets[30] suggested that the ultimate load is said to be reached when the equivalent plastic strain at any point of the numerical model reaches the true fracture strain of 100%. However, in the numerical simulations of CHS stub columns under combined tension and bending, it was generally found that the FE models underwent significant deformation and the cross-section shapes became increasingly oval after the maximum equivalent plastic strain reaches the true plastic strain of 40%. Therefore, the ultimate load was conservatively taken as the load corresponding to a maximum equivalent plastic strain of 40%. In total, 750 parametric study results were generated, with 250 for each of the three considered (austenitic, duplex and ferritic) stainless steel grades.

3 Assessment of Current Design Standards and Development of New Design Approaches

3.1 General

In this section, the existing design rules for stainless steel CHS under combined tension and bending moment, given in the European code EN 1993-1-4[18], American specification SEI/ASCE-8[19] and Australian/New Zealand standard AS/NZS 4673[20], are discussed and evaluated. The deformation-based continuous strength method[6–10] has been recently extended to cover the design of stainless steel CHS under combined compression and bending moment, and its applicability to the design of stainless steel CHS subjected to eccentric tension is also assessed herein. Table 2 reports the mean ratios of the numerical failure loads to the (unfactored) predicted failure loads $N_u/N_{u,pred}$ determined from each design method. A value of $N_u/N_{u,pred}$ ratio greater than unity indicates safe-sided resistance prediction.

3.2 European code EN 1993-1-4 (EC3)

The current European code EN 1993-1-4[18] employs nonlinear and linear interaction formulae for the design of Class 1 (or 2) and Class 3 stainless steel CHS subjected to combined tension and bending moment, as given by Eqs (5) and (6), respectively, where N_{Ed} is the design (applied) axial tensile load, $M_{Ed}=N_{Ed}e_0$ is the design (applied) bending moment, N_{Rd} is the cross-sectional tension resistance, and equal to the yield load, defined as the product of the gross section area A and the 0.2% proof stress $\sigma_{0.2}$, and M_{Rd} is the cross-sectional bending moment resistance, and taken as the plastic ($M_{pl}=W_{pl}\sigma_{0.2}$) and elastic ($M_{el}=W_{el}\sigma_{0.2}$) moment capacities for Class 1 (or 2) and Class 3 CHS, respectively, in which W_{pl} and W_{el} are the plastic and elastic section moduli, respectively, n is the ratio of the design axial tensile load to the cross-section yield load and $M_{R,pl}$ is the reduced plastic moment resistance to make allowance for the effect of the applied axial tensile load.

$$M_{R,pl} = M_{pl}(1 - n^{1.7}) \leq M_{pl} \tag{5}$$

$$\frac{N_{Ed}}{N_{Rd}} + \frac{M_{Ed}}{M_{Rd}} \leq 1 \tag{6}$$

The numerical results for austenitic, duplex and ferritic stainless steel CHS subjected to eccentric tension are normalised by the respective cross-section yield loads and plastic moment resistances, and plotted against the average EC3 linear and nonlinear design interaction curves in Figs 2(a)–2(c), respectively. The comparison results generally indicate an unduly higher level of scatter and conservatism of the EC3 resistance predictions for stainless steel CHS subjected to combined axial tension and bending moment. A quantitative evaluation of the EC3 resistance predictions is presented in Table 2, showing that the mean ratios of $N_u/N_{u,EC3}$ are equal to 1.47, 1.35 and 1.16, with the corresponding coefficient of variations (COVs) of 0.10, 0.12 and 0.12 for austenitic, duplex and ferritic stainless steel CHS subjected to eccentric tension, respectively. The conservatism and scatter of the EC3 predicted resistances result mainly from the inaccurate predictions of the tension and bending moment end points (i.e. cross-section resistances under pure tension and pure bending) of the design interaction curves, which are calculated without accounting for strain hardening, and thus limited to the cross-section yield loads and elastic (or plastic) moment resistances.

3.3 American specification SEI/ASCE-8

For the design of stainless steel CHS subjected to combined actions of axial compressive (or tensile) load and bending moment, the current American specification SEI/ASCE-8[19] employs a linear deign interaction curve, as defined by Eq. (7), where N_n and M_n are the cross-sectional resistances under tension and bending, respectively. The cross-sectional tension resistance N_n is equal to the yield load, while the bending moment resistance M_n, depending on the cross-section slenderness (diameter-to-thickness ratio D/t), is calculated from Eq. (8); for stocky CHS with D/t ratios less than $0.112E/\sigma_{0.2}$, M_n is taken as the elastic moment resistance (M_{el}) without considering the beneficial plasticity, while for slender CHS with D/t ratios greater than or equal to $0.112E/\sigma_{0.2}$, a reduced elastic moment resistance (K_cM_{el}) is adopted.

$$\frac{N_{Ed}}{N_n} + \frac{M_{Ed}}{M_n} \leq 1 \tag{7}$$

$$M_n = \begin{cases} M_{el} & \text{for } \dfrac{D}{t} \leq \dfrac{0.112E}{\sigma_{0.2}} \\ K_cM_{el} & \text{for } \dfrac{0.112E}{\sigma_{0.2}} < \dfrac{D}{t} \leq \dfrac{0.881E}{\sigma_{0.2}} \end{cases} \tag{8}$$

where K_c is the reduction factor, as defined by Eq. (9):

$$K_c = \frac{(1 - C)(E/\sigma_{0.2})}{(8.93 - \lambda_c)(D/t)} + \frac{5.882C}{8.93 - \lambda_c} \leq 1 \tag{9}$$

in which C is the ratio of the material effective proportional limit to the 0.2% proof stress, and λ_c = 3.048C is a material parameter.

The accuracy of the resistance predictions determined from the American specification SEI/ASCE-8[19] was evaluated through comparisons against the numerical ultimate failure loads. As can be seen from Table 2, the mean ratios of $N_u/N_{u,ASCE}$ are equal to 1.90, 1.75 and 1.48, with COVs of 0.10, 0.11 and 0.10, for austenitic, duplex and ferritic stainless steel CHS subjected to combined actions of axial tension and bending moment, respectively. The American specification SEI/ASCE-8[19] yields less accurate resistance predictions than the European code EN 1993-1-4[18], principally due to the adoption of a conservative linear design interaction curve for stainless steel CHS subjected to eccentric tension.

3.4 Australian/New Zealand standard AS/NZS 4673

The Australian/New Zealand standard AS/NZS 4673[20] adopts the same linear interaction formula for the design of stainless steel CHS subjected to eccentric tension as the American specification SEI/ASCE-8[19], as defined by Eq. (10), with the difference lying in the calculation of cross-section bending moment resistances, as given by Eq. (11). Specifically, the AS/NZS 4673 design provisions take into account the beneficial plasticity and allow the use of the plastic moment resistance for stocky CHS with D/t ratios less than $0.078E/\sigma_{0.2}$; the elastic moment resistance is used for non-slender CHS with D/t ratios greater than $0.078E/\sigma_{0.2}$ but less than $0.31E/\sigma_{0.2}$, while a reduced elastic moment resistance is adopted for slender CHS with D/t ratios greater than $0.31E/\sigma_{0.2}$. Note that the AS/NZS slenderness limit between slender and non-slender sections is equal to $0.31E/\sigma_{0.2}$, which is more favourable than the limit value of $0.112E/\sigma_{0.2}$, as specified in SEI/ASCE-8[19]. The reduction factor for elastic moment capacity K_a, as adopted in AS/NZS[20], differs from that used in SEI/ASCE-8[19], as given by Eq. (12).

$$\frac{N_{Ed}}{N_a} + \frac{M_{Ed}}{M_a} \leq 1 \tag{10}$$

$$M_a = \begin{cases} M_{pl} & \text{for } \dfrac{D}{t} < \dfrac{0.078E}{\sigma_{0.2}} \\ M_{el} & \text{for } \dfrac{0.078E}{\sigma_{0.2}} \leq \dfrac{D}{t} < \dfrac{0.31E}{\sigma_{0.2}} \\ K_a M_{el} & \text{for } \dfrac{0.31E}{\sigma_{0.2}} \leq \dfrac{D}{t} < \dfrac{0.881E}{\sigma_{0.2}} \end{cases} \tag{11}$$

$$K_a = \frac{(1-C)(E/\sigma_{0.2})}{(3.226-\lambda_c)(D/t)} + \frac{0.178\,C}{3.226-\lambda_c} \leq 1 \tag{12}$$

The accuracy of the Australian/New Zealand standard[20] was assessed by comparing the failure loads obtained from the numerical simulations with the AS/NZS resistance predictions. The mean $N_u/N_{u,AS/NZS}$ ratios, as reported in Table 2, are equal to 1.64, 1.49 and 1.28, with COVs of 0.09, 0.08 and 0.08 for austenitic, duplex and ferritic stainless steel CHS under combined axial tensile load and bending moment, respectively. The Australian/New Zealand standard AS/NZS 4673[20] was found to be more accurate than the American specification SEI/ASCE-8[19], owing to the use of more precise bending moment end point of the design interaction curve.

3.5 Continuous strength method (CSM)

The existing codified design interaction formulae for stainless steel CHS subjected to combined tension and bending moment yield conservative and scattered resistance predictions, due to the employment of linear interaction (except for EN 1993-1-4[18] for Class 1 and 2 sections) between axial tension and bending moment, without considering stress redistribution within stocky sections, and to the adoption of inaccurate end points, which are limited to the cross-section yield loads and elastic (or plastic) bending moment resistances, without accounting for strain hardening.

The continuous strength method (CSM)[7–10] is a deformation-based design approach and takes into account strain hardening in the determination of cross-section compression and bending moment resistances. For the design of stainless steel CHS under combined compression and bending moment (i.e. eccentric compression), Zhao et al.[6] proposed a simple but efficient design approach through the use of the EC3 linear and nonlinear design interaction curves but with the CSM cross-sectional capacities as the end points; the new design proposal was shown to yield a substantially higher level of design accuracy and consistency than the current international design codes. A brief summary of the CSM design proposal for stainless steel CHS under eccentric compression is described, and then its applicability to the design of stainless steel CHS subjected to eccentric tension is evaluated.

The use of the CSM requires firstly to identify the deformation capacity of a cross-section, which is achieved through the use of the CSM 'base curve'[7], as given by Eq. (13) for non-slender CHS, in which ε_{csm} is the maximum attainable compressive strain of a cross-section under the applied loading, ε_y is the yield strain, defined as $\sigma_{0.2}/E$, and $\bar{\lambda}_c = \sqrt{\sigma_{0.2}/\sigma_{cr}}$ is the cross-sectional slenderness, in which σ_{cr} is the cross-sectional elastic critical buckling stress under the applied loading. For CHS under isolated loading (pure compression and pure bending) and combined compression and bending, a unified expression is employed to determine the cross-sectional elastic local buckling stress σ_{cr}, as given by Eq. (14), where ν is the Poisson' ratio. With regards to the loading case of combined tension and bending moment, the favourable tension effect may lead to improved elastic local buckling stress. Moreover, for CHS under dominant tension load and low bending moment, tensile fracture may occur (i.e. no elastic local buckling stress). Extension of the CSM to cover the design of tension members is underway, while the unified expression, as given by Eq. (14), was employed herein to conservatively calculate the elastic critical stress of stainless steel CHS under combined tension and bending moment.

$$\frac{\varepsilon_{csm}}{\varepsilon_y} = \frac{4.44 \times 10^{-3}}{\bar{\lambda}_C^{\,4.5}} \text{ but} \leq min\left(15, \frac{C_1 \varepsilon_u}{\varepsilon_y}\right) \tag{13}$$

$$\sigma_{cr} = \frac{E}{\sqrt{3(1-\nu^2)}} \frac{2t}{D} \tag{14}$$

Upon determination of the cross-section limiting strain, an elastic, linear hardening material model is then adopted to enable the achievement of the design stresses greater than the 0.2% proof stress. The CSM material model features four coefficients (C_1, C_2, C_3 and C_4) and is depicted in Fig. 3, where C_1 is used to define a cut-off strain (see Eq. (13)), in order to avoid over-predicting failure strength from the CSM elastic, linear hardening model, C_2 is employed in Eq. (15) for the definition of strain hardening slope E_{sh}, and C_3 and C_4 are adopted to predict the strain at the material ultimate strength $\varepsilon_u = C_3(1-\sigma_{0.2}/\sigma_u)+C_4$. Values of the coefficients for various stainless steel grades were calibrated, on the basis of the material tensile coupon test data[8], and are reported in Table 3.

$$E_{sh} = \frac{\sigma_u - \sigma_{0.2}}{C_2 \varepsilon_u - \varepsilon_y} \tag{15}$$

The CSM design stress σ_{csm} is then determined by Eq. (16), while the CSM cross-section compression resistance $N_{csm,Rd}$ is equal to the CSM design stress σ_{csm} multiplied by the gross section area A, as given by Eq. (17), where γ_{M0} is a partial safety factor for cross-sectional resistance, with a recommended value of 1.1 for stainless steel. On the basis of the assumption of a linearly-varying through-depth strain distribution and the CSM bi-linear (elastic, linear hardening) material model, the resistance of a cross-section in bending $M_{csm,Rd}$ was firstly derived through numerical integration of the CSM design stress distribution throughout the cross-section depth, and then transformed into a simplified design formula, as given by Eq. (18)[7–10], where α is the CSM bending coefficient, and equals to 2.0 for CHS. Regarding the design of stainless steel CHS under combined compression and bending moment, Zhao et al.[6] proposed a simple but efficient approach through the use of the EC3 linear and nonlinear interaction curves but with the CSM compression and bending capacities as the end points, as given by Eqs (19) and (20) for $\bar{\lambda}_c > 0.27$and $\bar{\lambda}_c \leq 0.27$, respectively, where n_{csm} is the ratio of $N_{Ed}/N_{csm,Rd}$ and $M_{R,csm,Rd}$ is the reduced CSM bending moment capacity to make allowance for the effect of the applied axial load N_{Ed}. The applicability of this approach to the design of stainless steel CHS subjected to eccentric tension is then assessed. Note that development of the continuous strength method for the design of tension members is underway, and the CSM cross-section tension resistances were conservatively taken as the corresponding compression capacities herein.

$$\sigma_{csm} = \sigma_{0.2} + E_{sh}(\varepsilon_{csm} - \varepsilon_y) \tag{16}$$

$$N_{csm,Rd} = A\sigma_{csm} \tag{17}$$

$$M_{csm,Rd} = \frac{W_{pl}\sigma_{0.2}}{\gamma_{M0}}\left[1 + \frac{E_{sh}}{E}\frac{W_{el}}{W_{pl}}\left(\frac{\varepsilon_{csm}}{\varepsilon_y} - 1\right) - \left(1 - \frac{W_{el}}{W_{pl}}\right) \Big/ \left(\frac{\varepsilon_{csm}}{\varepsilon_y}\right)^{\alpha}\right] \tag{18}$$

$$\frac{N_{Ed}}{N_{csm,Rd}} + \frac{M_{Ed}}{M_{csm,Rd}} \leq 1 \qquad \text{for } \bar{\lambda}_c > 0.27 \tag{19}$$

$$M_{Ed} \leq M_{R,csm,Rd} = M_{csm,Rd}(1 - n_{csm}^{1.7}) \leq M_{csm,Rd} \qquad \text{for } \bar{\lambda}_c \leq 0.27 \tag{20}$$

The numerical results are normalised by the CSM tension and bending moment capacities, and plotted against the proposed linear and nonlinear design interaction curves, as depicted in Figs 4(a)–4(c). The comparison results generally reveal that the CSM design interaction curves yield a more accurate representation of the data points, in contrast to the EC3 design interaction curves, which lie well below the numerical results, as shown in Figs 2(a)–2(c). Note that the data points normalised by the CSM cross-sectional capacities in Figs 4(a)–4(c) are shown to be slightly scattered, especially for stainless steel CHS subjected to large tensile loads; this is mainly due to the conservative use of the CSM cross-sectional compression resistances as the corresponding tension capacities in the calculation. More consistent predictions of stainless steel CHS under combined tension and bending are expected to be achieved, upon the development of the CSM for tension members.

The accuracy of the CSM design proposals for stainless steel CHS subjected to eccentric tension is assessed through comparing the numerically derived failure loads against the predicted failure loads determined from Eqs (19) and (20). The mean ratios of numerical to CSM predicted failure loads $N_u/N_{u,csm}$, as reported in Table 2, are equal to 1.21, 1.17 and 1.10, and the corresponding COVs are equal to 0.10, 0.11 and 0.06 for austenitic, duplex and ferritic stainless steel CHS under combined axial tension and bending moment, respectively, indicating that the CSM design proposals result in a substantially higher level of design accuracy than the current international design standards; this is also evident in Figs 5–7, where the failure loads predicted from the CSM and the three aforementioned design standards are plotted against the numerical failure loads.

3.6 Summary

Overall, the American specification SEI/ASCER-8[19] leads to the most conservative resistance predictions for stainless steel CHS under combined tension and bending moment, due to the adoption of a linear design interaction curve anchored to conservative tension and bending moment end points, which are calculated without taking into account strain hardening. The Australian/New Zealand standard AS/NZS 4673[20] also employs a linear design interaction curve, but generally results in more accurate and consistent resistance predictions than the American specification SEI/ASCE-8[19], owing to the consideration of plasticity in the determination of cross-section bending moment resistances (i.e. more accurate bending moment end points). The European code EN 1993-1-4[18] adopts a nonlinear design interaction curve for stocky (Class 1 and 2) CHS under combined tension and bending moment, and yields the most accurate capacity predictions among the three international design standards. However, none of these codified design methods considers strain hardening, and therefore all lead to conservative resistance predictions of stainless steel CHS under eccentric tension. The CSM design proposals of adopting the EC3 linear and nonlinear interaction curves but with the CSM cross-sectional capacities as the end points are shown to result in a substantially higher level of design accuracy than the established design standards.

4 Reliability Analysis

Statistical analyses are performed to evaluate the reliability of the CSM design proposals for stainless steel CHS subject to combined axial tension and bending, based on a total of 750 numerical results, according to the EN 1990 requirements[32]. In the present reliability analysis, the material over-strength ratios for austenitic, duplex and ferritic stainless steels were respectively taken as 1.3, 1.1 and 1.2, with COVs equal to 0.06, 0.03 and 0.045, and the COV of the stainless steel cross-section geometric properties was equal to 0.050, following the recommendation by Afshan et al.[33]. Table 4 reports the key obtained statistical parameters, in which $k_{d,n}$ is the design fractile factor (ultimate limit state), b is the mean ratio of test and numerical resistances to design model resistances, V_δ is the COV of the tests and numerical simulations relative to the resistance model, V_r is the COV incorporating the uncertainties of model and basic variables, and γ_{M0} is the partial safety factor. The resulting partial factors for all the three stainless steel grades are less than the currently recommended value of 1.1 in EN 1993-1-4[18], therefore demonstrating the reliability of the CSM design proposals for stainless steel CHS subjected to combined tension and bending moment.

5 Conclusions

Finite element modelling and design of stainless steel CHS subjected to combined actions of axial tension and bending moment have been carried out. Numerical models were developed to simulate both the local buckling and fracture behaviour of stainless steel CHS under eccentric tension. The developed FE models were validated against the previous eccentric tension tests on CHS, and then employed to conduct parametric studies to generate structural performance data over a broad range of stainless steel grades, cross-section geometries and loading combinations. The derived FE results were employed to evaluate the accuracy of the established design provisions for stainless steel CHS under combined tension and bending moment given in the European code EN 1993-1-4[18], American specification SEI/ASCE-8[19] and Australian/New Zealand standard AS/NZS 4673[20]. Generally, all the three international design standards were found to yield conservative and scattered resistance predictions, due to the employment of linear design interaction curves (except for EN 1993-1-4[18] for Class 1 and 2 sections), without considering stress redistribution within stocky sections, and to the adoption of inaccurate end points, which were limited to the cross-section yield loads and elastic (or plastic) bending moment resistances, without accounting for strain hardening. The CSM design proposals adopt the EC3 linear and nonlinear interaction curves, but anchored to the more accurate tension and bending moment end points determined from the continuous strength method[6–10] to rationally consider strain hardening, and were shown to result in substantially improved predictions of resistances of stainless steel CHS subjected to eccentric tension. Finally, statistical analyses were performed to confirm the reliability of the CSM design proposals, according to the EN 1990 requirements[32].

References

[1] Zhao O, Rossi B, Gardner L, Young, B. Behaviour of structural stainless steel cross-sections under combined loading – Part I: Experimental study. Engineering Structures, 2015;89:236–46.

[2] Zhao O, Rossi B, Gardner L, Young B. Experimental and numerical studies of ferritic stainless steel tubular cross-sections under combined compression and bending. Journal of Structural Engineering (ASCE), 2016;142(2):04015110.

[3] Zhao O, Gardner L, Young B. Structural performance of stainless steel circular hollow sections under combined axial load and bending – Part 1: Experiments and numerical modelling. Thin-Walled Structures, 2016;101:231–9.

[4] Arrayago I, Real E. Experimental study on ferritic stainless steel RHS and SHS cross-sectional resistance under combined loading. Structures, 2015;4:69–79.

[5] Zhao O, Rossi B, Gardner L, Young B. Behaviour of structural stainless steel cross-sections under combined loading – Part II: Numerical modelling and design approach. Engineering Structures, 2015;89:247–59.

[6] Zhao O, Gardner L, Young B. Structural performance of stainless steel circular hollow sections under combined axial load and bending – Part 2: Parametric studies and design. Thin-Walled Structures, 2016;101:240–8.

[7] Afshan S, Gardner L. The continuous strength method for structural stainless steel design. Thin-Walled Structures, 2013;68(4):42–9.

[8] Buchanan C, Gardner L, Liew A. The continuous strength method for the design of circular hollow sections. Journal of Constructional Steel Research, 2016;118:207–16.

[9] Zhao O, Afshan S, Gardner L. Structural response and continuous strength method design of slender stainless steel cross-sections. Engineering Structures, 2017;140:14–25.

[10] Gardner L, Wang F, Liew A. Influence of strain hardening on the behavior and design of steel structures. International Journal of Structural Stability and Dynamics, 2011;11(05):855–75.

[11] Zhao O, Gardner L, Young B. Testing and numerical modelling of austenitic stainless steel CHS beam-columns. Engineering Structures, 2016;111:263–74.

[12] Lui WM, Ashraf M, Young B. Tests of cold-formed duplex stainless steel SHS beam–columns. Engineering structures, 2014;74:111–21.

[13] Huang Y, Young B. Experimental investigation of cold-formed lean duplex stainless steel beam-columns. Thin-Walled Structures, 2014;76:105–17.

[14] Zhao O, Gardner L, Young B. Buckling of ferritic stainless steel members under combined axial compression and bending. Journal of Constructional Steel Research, 2016;117:35–48.

[15] Zhao O, Gardner L, Young B. Experimental Study of Ferritic Stainless Steel Tubular Beam-Column Members Subjected to Unequal End Moments. Journal of Structural Engineering (ASCE), 2016; 142(11):04016091.

[16] Greiner R, Kettler M. Interaction of bending and axial compression of stainless steel members. Journal of Constructional Steel Research, 2008;64(11):1217–24.

[17] Zhao O, Gardner L, Young B. Behaviour and design of stainless steel SHS and RHS beam-columns. Thin-Walled Structures, 2016;106:330–45.

[18] EN 1993-1-4:2006+A1:2015. Eurocode 3: Design of steel structures – Part 1.4: General rules – Supplementary rules for stainless steels, including amendment A1 (2015). Brussels: European Committee for Standardization (CEN); 2015.

[19] SEI/ASCE 8-02. Specification for the design of cold-formed stainless steel structural members. Reston: American Society of Civil Engineers (ASCE); 2002.

[20] AS/NZS 4673. Cold-formed stainless steel structures. Sydney: AS/NZS 4673:2001; 2001.

[21] Hibbitt, Karlsson & Sorensen, Inc. ABAQUS. ABAQUS/Standard user's manual volumes I-III and ABAQUS CAE manual. Version 6.12. Pawtucket (USA); 2012.

[22] Ramberg W, Osgood WR. Description of stress–strain curves by three parameters. Technical note No 902, Washington DC: National advisory committee for aeronautics. 1943.

[23] Hill HN. Determination of stress–strain relations from offset yield strength values. Technical note No 927, Washington DC: National advisory committee for aeronautics. 1944.

[24] Mirambell E, Real E. On the calculation of deflections in structural stainless steel beams: An experimental and numerical investigation. Journal of Constructional Steel Research, 2000;54(1):109–33.

[25] Rasmussen KJR. Full-range stress-strain curves for stainless steel alloys. Journal of Constructional Steel Research, 2003;59(1):47–61.

[26] Gardner L, Nethercot DA. Experiments on stainless steel hollow sections—Part 1: Material and cross-sectional behaviour. Journal of Constructional Steel Research, 2004;60(9):1291–318.

[27] Afshan S, Rossi B, Gardner L. Strength enhancements in cold-formed structural sections – Part I: Material testing. Journal of Constructional Steel Research, 2013;83:177–88.

[28] Dowling NE. Mechanical behaviour of materials. New Jersey (USA): Prentice Hall; 1999.

[29] Zhang Z L, Hauge M, Ødegård J, Thaulow C. Determining material true stress–strain curve from tensile specimens with rectangular cross-section, International Journal of Solids Structures. 1999;36:3497–516.

[30] Salih EL, Gardner L, Nethercot DA. Numerical investigation of net section failure in stainless steel bolted connections. Journal of Constructional Steel Research, 2010;66(12):1455–66.

[31] Li W, Han LH, Chan TM. Performance of concrete-filled steel tubes subjected to eccentric tension. Journal of Structural Engineering, 2015;141(12):04015049.

[32] EN 1990. Eurocode – basis of structural design. Brussels: European Committee for Standardization (CEN); 2002.

[33] Afshan S, Francis P, Baddoo NR, Gardner L. Reliability analysis of structural stainless steel design provisions. Journal of Constructional Steel Research, 2015;114:293–304.

6 Figures

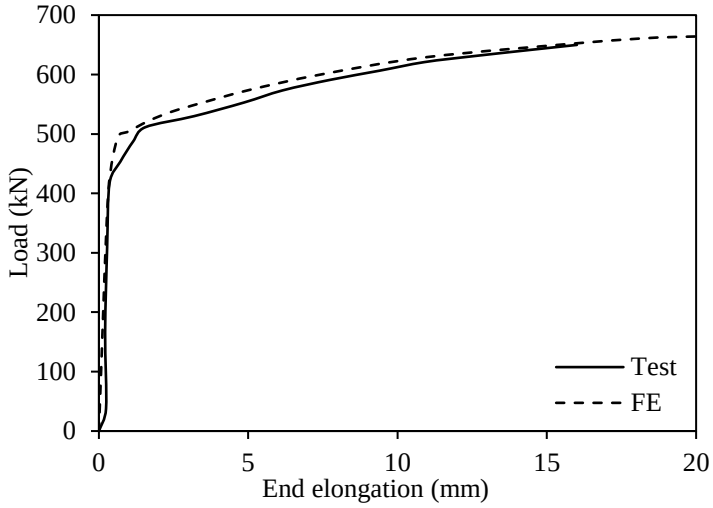

(a) CHS 140×3 (e_0=0 mm)

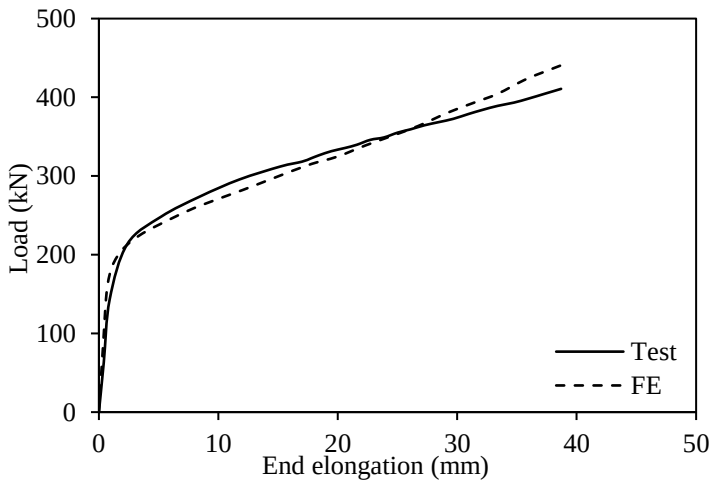

(b) CHS 140×3 (e_0=70 mm)

Fig. 1 Experimental and numerical load–end elongation curves for typical CHS stub column specimens[31] under eccentric tension

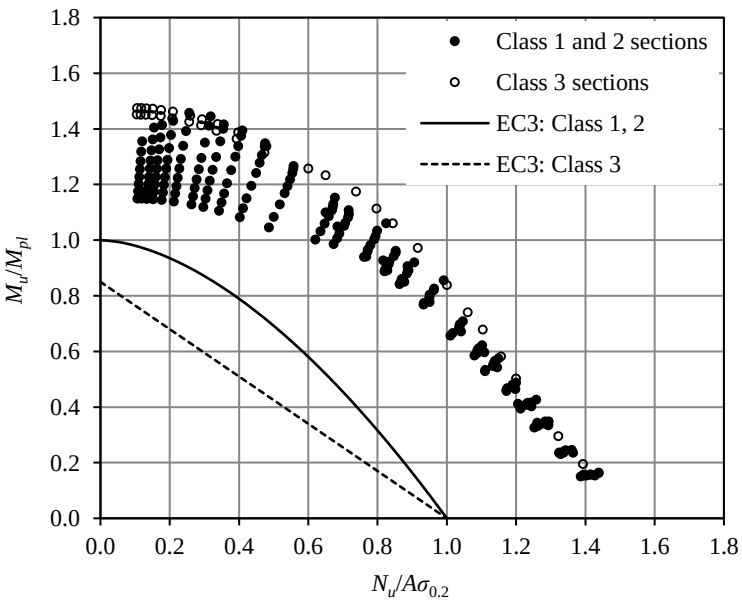

(a) Austenitic stainless steel

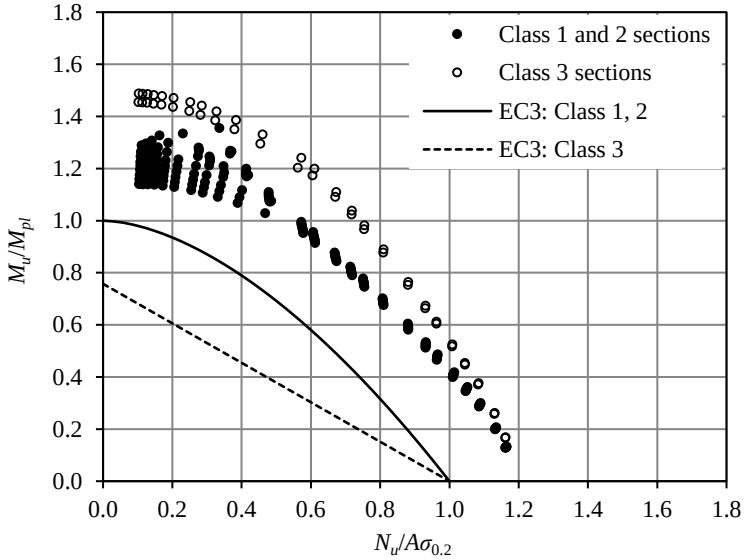

(b) Duplex stainless steel

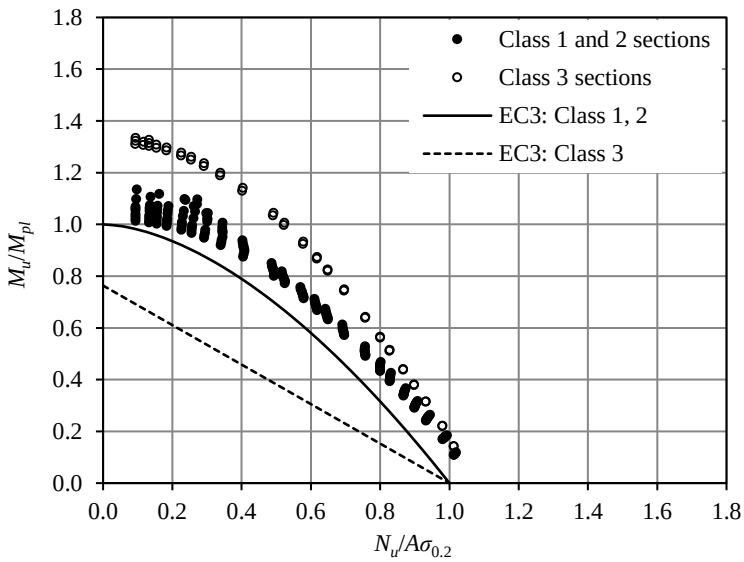

(c) Ferritic stainless steel

Fig. 2 Eccentric tension FE results normalised by the plastic moment capacity and yield load (i.e. the EC3 end points for Class 1 and 2 cross-sections)

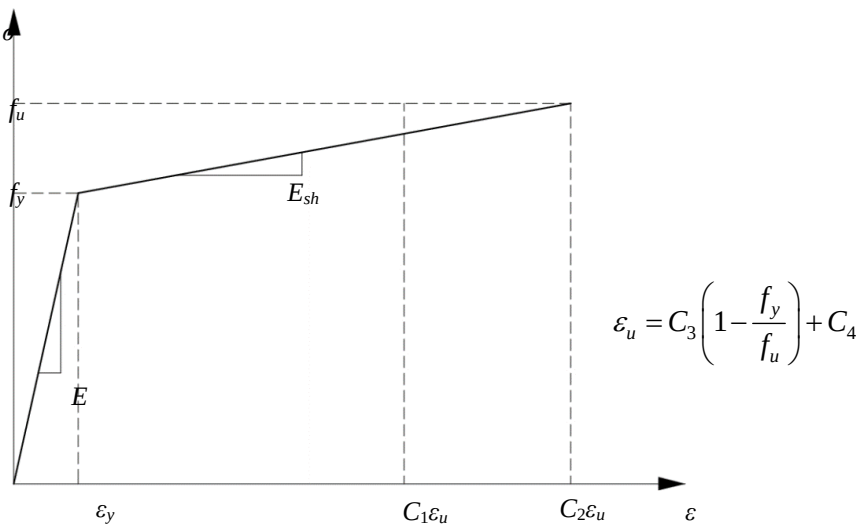

Fig. 3 CSM elastic, linear hardening material model

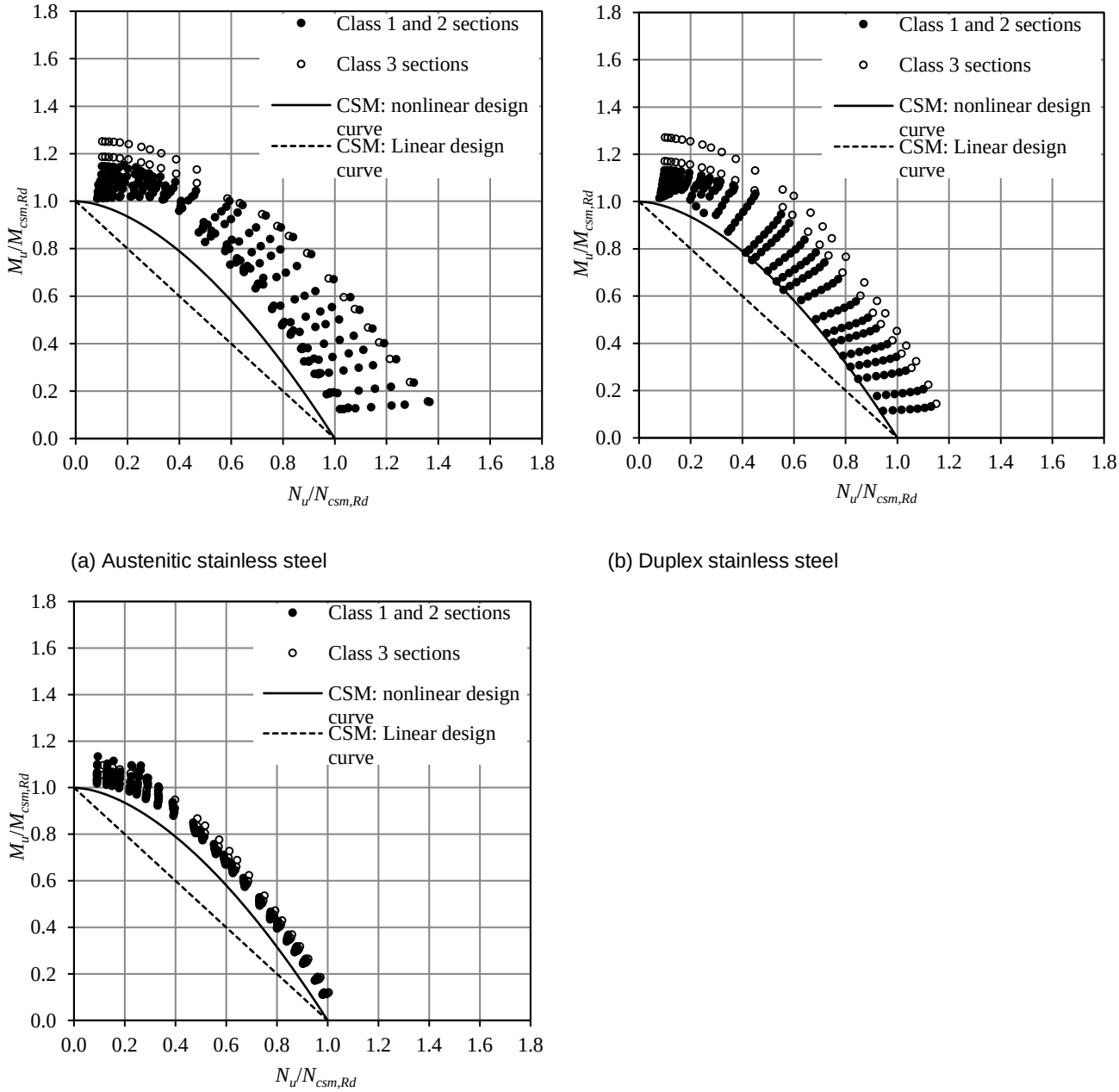

(a) Austenitic stainless steel

(b) Duplex stainless steel

(c) Ferritic stainless steel

Fig. 4 Eccentric tension FE results normalised by CSM cross-sectional capacities

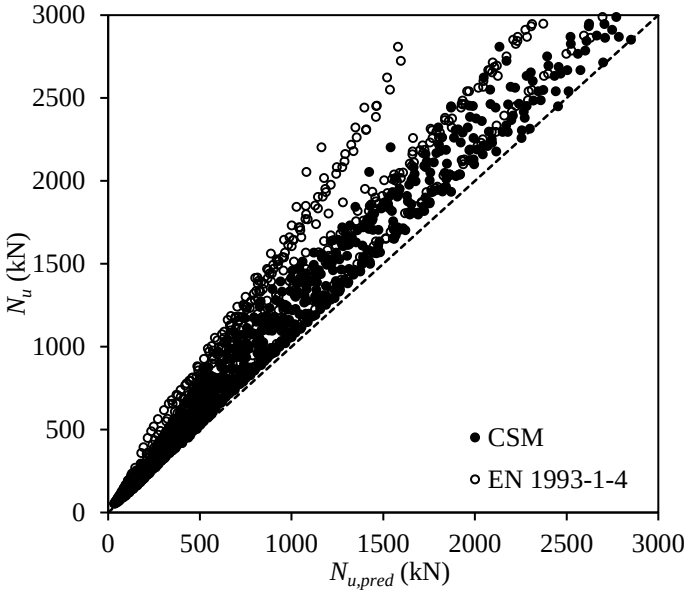

Fig. 5 Comparison of test and FE results with CSM and EN 1993-1-4 strength predictions

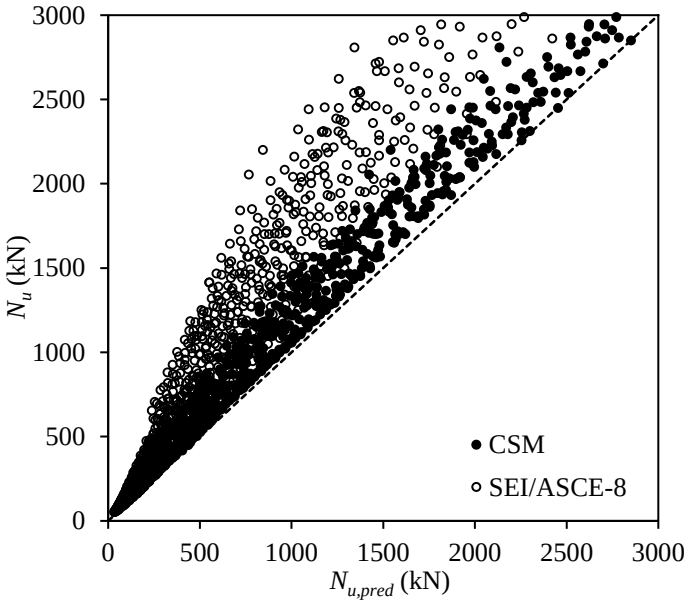

Fig. 6 Comparison of test and FE results with CSM and SEI/ASCE-8 strength predictions

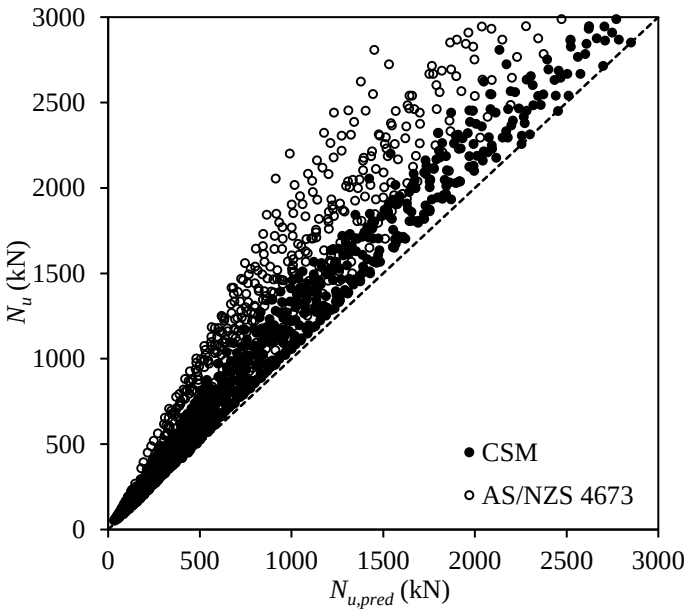

Fig. 7 Comparison of test and FE results with CSM and AS/NZS strength prediction

7 Tables

Table 1 Summary of key material properties employed in the FE models

Material grade	E	$\sigma_{0.2}$	$\sigma_{1.0}$	σ_u	R-O coefficients	
	(N/mm²)	(N/mm²)	(N/mm²)	(N/mm²)	n	m
Austenitic	190000	355	396	780	5.3	1.9
Duplex	198000	635	694	756	6.0	4.0
Ferritic	199000	470	485	488	7.3	10.9

Table 2 Comparisons of numerical results of stainless steel CHS under eccentric tension with predicted resistance

Material grade	No. of FE data		$N_u/N_{u,EC3}$	$N_u/N_{u,ASCE}$	$N_u/N_{u,AS/NZS}$	$N_u/N_{u,csm}$
Austenitic	250	Mean	1.47	1.90	1.64	1.21
		COV	0.10	0.10	0.09	0.10
Duplex	250	Mean	1.35	1.75	1.49	1.17
		COV	0.12	0.11	0.08	0.11
Ferritic	250	Mean	1.16	1.48	1.28	1.10
		COV	0.12	0.10	0.08	0.06

Table 3 Summary of the CSM material model coefficients for each stainless steel grade

Material grade	C_1	C_2	C_3	C_4
Austenitic	0.10	0.16	1.00	0
Duplex	0.10	0.16	1.00	0
Ferritic	0.40	0.45	0.60	0

Table 4 Reliability analysis results calculated according to EN 1990

Material grade	No. of FE data	$k_{d,n}$	b	V_δ	V_r	γ_{M0}
Austenitic	250	3.130	1.159	0.094	0.122	0.98
Duplex	250	3.130	1.099	0.103	0.118	1.09
Ferritic	250	3.130	1.076	0.054	0.086	1.01